

# Characterization of reactive oxidized nitrogen in the global upper troposphere using recent and historic commercial and research aircraft campaigns and GEOS-Chem

5 Nana Wei<sup>1</sup>, Eloise A. Marais<sup>1</sup>, Gongda Lu<sup>1\*</sup>, Robert G. Ryan<sup>1\*\*</sup>, Bastien Sauvage<sup>2</sup>

<sup>1</sup> Department of Geography, University College London, London, UK.

<sup>2</sup> Laboratoire d'Aérodynamique, Université de Toulouse, CNRS, Université Toulouse III Paul Sabatier, France.

\* Now at: the Satellite Application Center for Ecology and Environment, Ministry of Ecology and Environment, Beijing, China.

10 \*\* Now at: School of Geography, Earth and Atmospheric Science, University of Melbourne, Melbourne, Australia.

Correspondence to: Nana Wei ([nana.wei.21@ucl.ac.uk](mailto:nana.wei.21@ucl.ac.uk)); Eloise A. Marais ([e.marais@ucl.ac.uk](mailto:e.marais@ucl.ac.uk))

**Abstract.** Reactive oxidized nitrogen (NO<sub>y</sub>) in the upper troposphere (UT) influences global climate, air quality, and tropospheric oxidants, but this is informed by limited knowledge of the relative contribution of individual  
15 NO<sub>y</sub> components in this undersampled layer. Here we use sporadic NASA DC-8 aircraft campaign observations, after screening for plumes and stratospheric influence, to characterise UT NO<sub>y</sub> composition and evaluate current knowledge of UT NO<sub>y</sub> as simulated with the GEOS-Chem model. Use of DC-8 data follows confirmation that these intermittent data reproduce NO<sub>y</sub> seasonality from routine commercial aircraft observations (2003-2019), supporting use of DC-8 data to characterize UT NO<sub>y</sub>. We find that peroxyacetyl nitrate (PAN) dominates UT NO<sub>y</sub>  
20 (30-64% of NO<sub>y</sub>), followed by nitrogen oxides (NO<sub>x</sub> ≡ NO + NO<sub>2</sub>) (6-18%), peroxyacetic acid (HNO<sub>3</sub>) (6-13%), and nitric acid (HNO<sub>3</sub>) (7-11%). Methyl peroxy nitrate (MPN) makes an outsized contribution to NO<sub>y</sub> (14-24%) over the Southeast US relative to the other regions sampled (2-7%). GEOS-Chem, sampled along DC-8 flights, exhibits much weaker seasonality than DC-8, underestimating summer and spring NO<sub>y</sub> and overestimating winter and autumn NO<sub>y</sub>. The model consistently overestimates peroxypropionyl nitrate (PPN) by ~10-16 pptv or 10%-  
25 90% and underestimates NO<sub>2</sub> by 6-36 pptv or 31%-65%, as the model is missing PPN photolysis. A model underestimate in MPN of at least ~50 pptv (13-fold) over the Southeast US results from uncertainties in processes that sustain MPN production as air ages. Our findings highlight that greater understanding of UT NO<sub>y</sub> is critically needed to determine its role in the nitrogen cycle, air pollution, climate, and abundance of oxidants.

## 1 Introduction

30 Reactive oxidized nitrogen (NO<sub>y</sub>) in the upper troposphere impacts global climate, surface air quality and the oxidizing capacity of the whole troposphere (Mickley et al., 1999; Bradshaw et al., 2000; Dahlmann et al., 2011; Worden et al., 2011). NO<sub>y</sub> is an important climate driver because tropospheric ozone (O<sub>3</sub>) production is limited by the availability of NO<sub>y</sub>, particularly in the upper troposphere where the radiative forcing efficiency of O<sub>3</sub> peaks (Dahlmann et al., 2011; Worden et al., 2011; Rap et al., 2015). Influence on tropospheric O<sub>3</sub> production also  
35 affects abundance of the main atmospheric oxidant, the hydroxyl radical (OH), thus altering the lifetimes of the longer-lived greenhouse gas methane and the air pollutants carbon monoxide (CO) and volatile organic compounds (VOCs) (Murray et al., 2013; Seltzer et al., 2015).

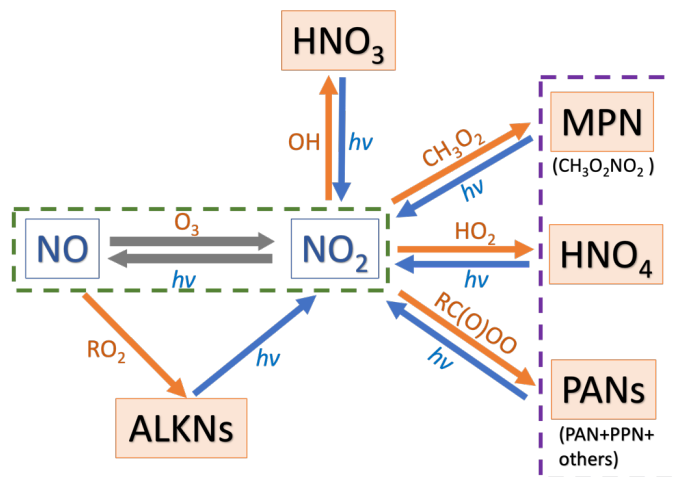
Knowledge of dominant daytime  $\text{NO}_y$  compounds, sources, chemistry, fate, and persistence in the upper troposphere has been largely informed by observations and models used as part of research and commercial aircraft campaigns (Boersma et al., 2011; Marais et al., 2018; Silvern et al., 2018; Travis et al., 2016; 2020). Instruments onboard research aircraft that sample the upper troposphere, in particular the recently retired NASA DC-8 platform, have undergone substantial development to directly measure and derive estimates of a large suite of upper tropospheric  $\text{NO}_y$  compounds. These include nitrogen oxides ( $\text{NO}_x \equiv \text{NO} + \text{NO}_2$ ), peroxyacetyl nitrate (PAN) and other prominent PAN-type compounds, nitric acid ( $\text{HNO}_3$ ), peroxyxynitric acid ( $\text{HNO}_4$ ), alkyl nitrates (ALKNs) and, more recently, methyl peroxy nitrate (MPN).

These aircraft campaigns have confirmed that sources of  $\text{NO}_y$  to the upper troposphere are dominated by lightning  $\text{NO}_x$  emissions (Levy II et al., 1999; Gressent et al., 2014; 2016; Marais et al., 2018), causing a seasonal maximum in  $\text{NO}_y$  in summer months and a minimum in winter in parts of the world such as the northern midlatitudes where there is large seasonal variability in lightning activity (Blakeslee et al., 2014; Stratmann et al., 2016). Other  $\text{NO}_y$  source contributors include  $\text{NO}_x$  emissions from cruising altitude aircraft (Brasseur et al., 1996), stratospheric downwelling of air masses laden with  $\text{HNO}_3$  and  $\text{NO}_2$  that also promote prompt formation of PANs on mixing with cold upper tropospheric air (Levy II et al., 1980; Jacob et al., 2010; Liang et al., 2011), deep convective uplift of surface pollution (Ehhalt et al., 1992; Jaeglé et al., 1998; Bertram et al., 2007), and aged air masses initially very photochemically active that accumulate MPN (Nault et al., 2015).

Chemical cycling of dominant daytime  $\text{NO}_y$  components, informed by past review and measurement compilation studies of the free troposphere (Emmons et al., 1997; Bradshaw et al., 2000), is illustrated in Figure 1. During the day,  $\text{NO}$  and  $\text{NO}_2$  are in photostationary steady state, as  $\text{NO}$  oxidation, mostly by  $\text{O}_3$ , is balanced by  $\text{NO}_2$  photolysis.  $\text{NO}_x$  also reacts to form reservoir compounds. For  $\text{NO}_2$ , these include  $\text{HNO}_3$  from reaction with  $\text{OH}$ , PANs from reaction with peroxy acyl radicals ( $\text{RC(O)OO}\cdot$ ),  $\text{HNO}_4$  from reaction with the hydroperoxyl radical ( $\text{HO}_2\cdot$ ), and MPN from reaction with the methyl peroxy radical ( $\text{CH}_3\text{O}_2\cdot$ ). PANs in the upper troposphere are typically dominated by PAN followed by peroxypropionyl nitrate (PPN) (Singh, 1987; Roberts, 1990; 1998; 2002). For  $\text{NO}$ , reservoir compounds include ALKNs from reaction with non-acyl peroxy radicals ( $\text{RO}_2\cdot$ ). Recycling of reservoir compounds back to  $\text{NO}_x$  is dominated by photolysis, as thermally labile peroxy nitrates (PNs) including PANs,  $\text{HNO}_4$  and MPN are stable against decomposition in the cold upper troposphere (Huey, 2007). This recycling along with  $\text{NO}_y$  sources to the upper troposphere sustains upper tropospheric  $\text{NO}_x$  concentrations at  $\sim 30$  pptv over the remote ocean and  $\sim 100$  pptv over polluted landmasses (Marais et al., 2018; 2021; Shah et al., 2023). Stable  $\text{NO}_x$  reservoir compounds are transported long distances before subsiding and decomposing on warming, thus supplying other parts of the world with oxidants ( $\text{HO}_x$ ) and  $\text{O}_3$  precursors ( $\text{NO}_x$  and peroxy radicals) (Schultz et al., 1999). Loss processes in the dry upper troposphere are slow and dominated by subsidence, resulting in long  $\text{NO}_y$  lifetimes of 10-20 days (Logan, 1983; Prather and Jacob, 1997). Similarly,  $\text{NO}_x$  has a lifetime of about a week compared to less than a day in the boundary layer ( $< 2$  km) (Jaeglé et al., 1998).

Nighttime  $\text{NO}_y$  chemistry is also important, but aircraft campaign measurements of the nocturnal upper troposphere are mostly of total  $\text{NO}_y$  from commercial aircraft campaigns. The nighttime chemistry not in Figure 1 includes  $\text{NO}$  reaction with  $\text{OH}$  forming nitrous acid ( $\text{HONO}$ ) that accumulates in the absence of photolysis, as

75 well as  $\text{NO}_2$  reaction with  $\text{O}_3$  to form the nitrate radical ( $\text{NO}_3$ ) that further reacts with  $\text{NO}_2$  to produce  $\text{N}_2\text{O}_5$ , a precursor of aerosol nitrate ( $\text{pNO}_3$ ) (Bradshaw et al., 2000).



80 **Figure 1: Dominant daytime reactive oxidized gas-phase nitrogen components and reaction pathways in the upper troposphere. Arrow colours distinguish formation (orange) and photolytic ( $h\nu$ ) decomposition (blue) of reservoir compounds. Dashed boxes indicate compounds of the  $\text{NO}_x$  family (green) and classed as peroxy nitrates (purple). "R" in  $\text{RC(O)OO}$  and  $\text{RO}_2$  represents an alkyl group.**

Modelling studies evaluating best understanding of  $\text{NO}_y$  in the upper troposphere routinely identify stark discrepancies between observed and modelled total  $\text{NO}_y$ ,  $\text{NO}_x$ , and the ratio of  $\text{NO}$ -to- $\text{NO}_2$  in the upper layers of the troposphere (Jaeglé et al., 1998; Talbot et al., 1999; Bertram et al., 2007; Hudman et al., 2007; Liang et al., 2011; Nault et al., 2015; Huntrieser et al., 2016; Travis et al., 2016; Fisher et al., 2018; Silvern et al., 2018; Lee et al., 2022; Cohen et al., 2023). These studies have either focused on a few  $\text{NO}_y$  components, or a single aircraft campaign. A more holistic investigation of all  $\text{NO}_y$  components is needed, as is advocated by Murray et al. (2021), to reduce uncertainties in knowledge of the current, past, and potential future abundances of tropospheric oxidants. Past studies have also documented the challenges examining measurements made in the upper troposphere. These include screening for stratospheric influence, determining the height of the chemical tropopause, and selecting observations and campaigns that are climatologically representative of a standard atmosphere (Weinheimer et al., 1994; Fuelberg et al., 2000; Bertram et al., 2007; Barth et al., 2015; Huntrieser et al., 2016). Instruments measuring  $\text{NO}_2$  are also susceptible to interference from decomposition of the least thermally stable  $\text{NO}_x$  reservoir compounds,  $\text{HNO}_4$  and  $\text{MPN}$ , that are abundant in the cold upper troposphere (Ryerson et al., 2000; Shah et al., 2023).  $\text{NO}_y$  from these same instruments can also be biased by decomposition of non- $\text{NO}_y$  fixed nitrogen compounds prevalent in the upper troposphere, such as hydrogen cyanide ( $\text{HCN}$ ) (Bradshaw et al., 1998).

Here we use NASA DC-8 research and IAGOS commercial aircraft campaign measurements, each spanning more than a decade, to characterize global  $\text{NO}_y$  seasonality and composition in the upper troposphere. This follows careful campaign and data selection to isolate observations sampling the upper troposphere under standard

100 conditions for broad assessment of consistent NO<sub>y</sub> seasonality between DC-8 and routine commercial aircraft  
campaign observations. We go on to use the DC-8 data to critique contemporary understanding of upper  
tropospheric NO<sub>y</sub> as simulated by the GEOS-Chem model.

## 2 Materials and methods

### 105 2.1 Research aircraft observations of total and components of NO<sub>y</sub>

The DC-8 research aircraft has sampled ambient air covering the near full extent of the troposphere since its  
maiden campaign in 1985 (Culter, 2009). Many of the initial campaigns included instruments that measured a  
subset of the NO<sub>y</sub> components shown in Figure 1, typically continuous measurements of total NO<sub>y</sub>, NO, HNO<sub>3</sub>,  
PAN and PPN, and whole air sampler (WAS) collection and laboratory detection of C1-C5 ALKs (Singh et al.,  
110 1999). Since 2004, DC-8 campaigns have included continuous measurements of HNO<sub>4</sub>, other PAN-type species  
and total PNs (Singh et al., 2006). Given this, we only consider DC-8 campaigns with a relatively consistent suite  
of instruments that mostly sampled well-mixed air representative of a climatologically standard atmosphere. These  
criteria eliminate the summer 2004 Intercontinental Chemical Transport Experiment-North America (INTEX-NA)  
campaign (Singh et al., 2006; Singh et al., 2009) that is the only DC-8 campaign since 2004 to not include a NO<sub>x</sub>  
115 and NO<sub>y</sub> chemiluminescence analyzer, and the summer 2012 Deep Convective Clouds and Chemistry (DC3)  
campaign that targeted convective thunderstorms influenced by fresh surface pollution and lightning NO<sub>x</sub>  
emissions (Barth et al., 2015).

The DC-8 campaigns we use are the Arctic Research of the Composition of the Troposphere from Aircraft and  
Satellites (ARCTAS) over the Arctic and sub-Arctic in spring and summer 2008 (Jacob et al., 2010), the Studies  
120 of Emissions and Atmospheric Composition, Clouds and Climate Coupling by Regional Surveys (SEAC<sup>4</sup>RS) over  
the Southeast US in late summer and early autumn 2013 (Toon et al., 2016), the Korea-United States Air Quality  
(KORUS-AQ) over South Korea in late spring and early summer 2016 (Crawford et al., 2021), and the  
Atmospheric Tomography Mission (ATom) that included 4 sub-campaigns along the same flight path from pole  
to pole over the Atlantic and Pacific Oceans in all 4 seasons from 2016 to 2018 (Thompson et al., 2021). ATom  
125 sub-campaigns are ATom-1 in July-August, ATom-2 in January-February, ATom-3 in September-October and  
ATom-4 in April-May. The data for these campaigns are from NASA data portals for each campaign downloaded  
as merged 1-minute files for ARCTAS (NASA, 2009), SEAC<sup>4</sup>RS (NASA, 2015) and KORUS-AQ (NASA, 2017)  
and as two separate merged files for ATom with the WAS C1-C5 ALKs data at variable time intervals of 40 s,  
1 min and 2 min and without the WAS C1-C5 ALKs data at 1-minute resolution (NASA, 2021).

130 Figure 2 shows the global sampling extent of the upper troposphere by NASA DC-8 after applying filtering criteria  
to the data to isolate observations representative of photochemical steady-state conditions. For this, we select  
daytime (08h30-15h30 local solar time or LST) observations within a wide pressure range from 180 hPa (~8 km)  
to the DC8 ceiling of 450 hPa (~12 km). This captures the full vertical extent of the midlatitude upper troposphere,  
but not the tropics. The tropical tropopause, according to NASA Modern-Era Retrospective analysis for Research  
135 and Applications version 2 (MERRA-2) meteorology, extends to ~16 km. We separate the stratosphere from the  
troposphere with a tropopause definition that can be applied to all datasets. We remove data with observed O<sub>3</sub>

concentrations above thresholds that represent the location of the chemical tropopause (Zahn et al., 2002). The thresholds we use are a single year-round value for the tropics (20°N to 20°S) of 100 ppbv (Dameris, 2015) and seasonally varying values everywhere else calculated using the day-of-year dependent O<sub>3</sub> tropopause equation derived by Zahn et al. (2002) from the inverse relationship between O<sub>3</sub> and CO observations from commercial aircraft campaigns. These are 120 ppbv in spring, 103 ppbv in summer, 74 ppbv in autumn, and 91 ppbv in winter. We also screen for stratospheric intrusions (identified as observations with O<sub>3</sub>/CO > 1.25 mol mol<sup>-1</sup>) (Hudman et al., 2007), fresh NO<sub>x</sub> emissions (NO<sub>y</sub>/NO < 3 mol mol<sup>-1</sup>), fresh convection (large (> 10 nm diameter) condensation nuclei > 10<sup>4</sup> cm<sup>-3</sup>), biomass burning plumes (CO > 200 ppbv and acetonitrile > 200 pptv) (Shah et al., 2023), as well as instances where NO<sub>2</sub> photolysis frequencies are approximately zero. The latter removes high latitude ATom measurements obtained at 08h30-15h30 LST under dark conditions during polar twilight or polar night. The data that are retained correspond to solar zenith angles ≤ 80° in polar regions, and ≤ 60° at other latitudes. The proportion of observations at 450-180 hPa is 42-50% for ATom and 16-37% for the other campaigns. After applying all other data screening, 20% of all data are retained for ATom and 7-11% for the other campaigns.

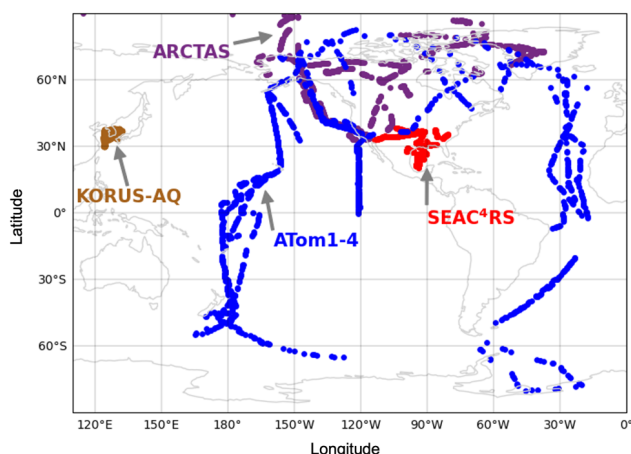
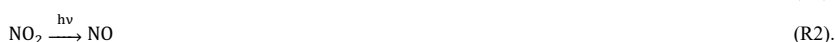


**Figure 2: Extent of NASA DC-8 sampling of the upper troposphere under standard, steady-state conditions. Colours distinguish ARCTAS (plum), SEAC<sup>4</sup>RS (red), KORUS-AQ (brown), and ATom (blue). ATom points are the 1-minute resolution data.**

The DC-8 instruments measuring NO<sub>y</sub> components (Figure 1) that are common to all campaigns include a chemiluminescence instrument measuring NO, NO<sub>2</sub>, and total NO<sub>y</sub> (Ryerson et al., 2000; Pollack et al., 2010; Bourgeois et al., 2022), a chemical ionization mass spectrometer (CIMS) measuring HNO<sub>3</sub> (Crounse et al., 2006), a CIMS measuring HNO<sub>4</sub>, PAN, PPN, and other PANs (Huey, 2007), and a Whole Air Sampler (WAS) collecting samples analysed in the laboratory using gas chromatography with flame ionization and atomic emission to detect C1-C5 ALKNs (Blake et al., 2003). The other PANs measured with the CIMS include peroxyacryloyl nitrate (APAN), peroxyisobutyryl nitrate (PiBN), peroxybutyryl nitrate (PBN), and peroxybenzoyl nitrate (PBZN). Other instruments deployed for select campaigns are Thermal-Dissociation Laser Induced Fluorescence (TD-LIF) measuring NO<sub>2</sub>, total PNs and total ALKNs (ARCTAS, KORUS-AQ, SEAC<sup>4</sup>RS) (Day et al., 2002) and the PAN

and Trace Hydrohalocarbon Experiment (PANTHER) instrument measuring PAN (ATom). There are also TD-LIF methyl peroxy nitrate (MPN) measurements reported in the SEAC<sup>4</sup>RS dataset and derived for ARCTAS by Browne et al. (2011).

Concentrations of NO<sub>2</sub> in the upper troposphere are close to chemiluminescence instrument uncertainty (Pollack et al., 2010; Bourgeois et al., 2022) and the measurements include interference from decomposition of NO<sub>x</sub> reservoir compounds in the instrument inlet. The Reed et al. (2016b) temperature-dependent inlet temperature decomposition profiles of individual NO<sub>x</sub> reservoir compounds for an instrument similar to that operated on the DC-8 suggests interference of 80-100% MPN and 15-45% HNO<sub>4</sub> for the typical inlet temperature range of the DC-8 chemiluminescence instrument of 20-30°C (Bourgeois et al., 2022). For the campaigns that measured HNO<sub>4</sub> and derived or measured MPN, this amounts to 13-27 pptv for ARCTAS and 71-92 pptv for SEAC<sup>4</sup>RS. Given this, we instead calculate NO<sub>2</sub> using the NO-NO<sub>2</sub> photochemical steady state (PSS) approximation, as is now standard (Travis et al., 2016; Shah et al., 2023; Horner et al., 2024). Conversion of NO to NO<sub>2</sub>, mostly (75%) due to oxidation by O<sub>3</sub> in the upper troposphere (Silvern et al., 2018), is balanced by NO<sub>2</sub> photolysis back to NO:



As NO<sub>x</sub> is in steady state for the daylight observations we isolate, NO<sub>2</sub> can be calculated as follows:

$$\text{NO}_2 = \text{NO} \times \left( \frac{k_1[\text{O}_3] + k_2[\text{HO}_2] + k_3[\text{BrO}]}{j_{\text{NO}_2}} \right) \quad (1).$$

Compounds in square brackets are in molecules cm<sup>-3</sup>. NO and NO<sub>2</sub> are in pptv. Terms not introduced yet include the NO<sub>2</sub> photolysis frequency,  $j_{\text{NO}_2}$ , in s<sup>-1</sup>, bromine monoxide (BrO), and rate constants of NO oxidation (R1) ( $k_{1-3}$ ), in cm<sup>3</sup> molecule<sup>-1</sup> s<sup>-1</sup>. Temperature-dependent values of  $k_{1-3}$  are those recommended by the Jet Propulsion Laboratory (JPL) (Burkholder, 2020), calculated using DC-8 ambient temperature measurements. NO, [O<sub>3</sub>], and  $j_{\text{NO}_2}$  are from the DC-8 measurements and [HO<sub>2</sub>] is from the DC-8 measurements for all campaigns, except SEAC<sup>4</sup>RS when it was not measured. We use GEOS-Chem (detailed in Sect. 2.3) simulated [HO<sub>2</sub>] to estimate SEAC<sup>4</sup>RS PSS NO<sub>2</sub>. [BrO] is from GEOS-Chem for all campaigns. NO is also converted to NO<sub>2</sub> by organic peroxy radicals (RO<sub>2</sub>), but we ignore this reaction as it is relatively insignificant throughout the free troposphere (Shah et al., 2023).

The NO<sub>y</sub> components not measured during specific campaigns are inferred. These include HNO<sub>4</sub> for KORUS-AQ, and ATom-3-4, PPN for ATom-1-2, and MPN for ARCTAS, ATom-1-4 and KORUS-AQ. The approaches used to infer these values differs, informed by the results, so a detailed description of this inference is in Section 3.2.

## 2.2 Commercial aircraft observations of total NO<sub>y</sub>

We use routine observations of upper tropospheric total NO<sub>y</sub> from instruments on commercial long-haul passenger aircraft to determine if the intermittency and brevity of DC-8 campaign observations are representative of climatological conditions. The In-service Aircraft for a Global Observing System (IAGOS) European research infrastructure (Boulanger et al., 2018) provides routine in situ measurements of NO<sub>y</sub> (Petzold et al., 2015). These are available from two IAGOS programmes: the Measurement of Ozone and Water Vapor by Airbus In-Service Aircraft (MOZAIC) (Marenco et al., 1998) from 2001 to 2005 (Volz-Thomas et al., 2005) and the Civil Aircraft for the Regular Investigation of the Atmosphere Based on an Instrument Container (CARIBIC) since December 2004 (Brenninkmeijer et al., 2007; Stratmann et al., 2016).

We consider the MOZAIC and CARIBIC observations together (collectively named IAGOS), as both programmes employed a chemiluminescence instrument with the same NO<sub>y</sub> detection technique (Volz-Thomas et al., 2005; Brenninkmeijer et al., 2007). Direct intercomparison of NO<sub>y</sub> is not possible, as there is no overlap in MOZAIC and CARIBIC NO<sub>y</sub>. Data from 2003 to 2019 are used; 2003-2005 for MOZAIC and 2005-2019 for CARIBIC. We isolate daytime, upper tropospheric observations by applying the same O<sub>3</sub> tropopause, stratospheric O<sub>3</sub> intrusion, and daytime filtering as is applied to DC-8 data (Sect. 2.1) using IAGOS O<sub>3</sub> and CO measurements. There are no NO<sub>2</sub> photolysis frequency measurements, but the requirement for spatial coincidence with ATom excludes polar twilight and night measurements at high latitudes. We do not screen for observations impacted by fresh emissions, vertical convection or biomass burning plumes, due to unavailability of concurrent measurements of suitable chemical tracers in the IAGOS data. As we consider 17 years of IAGOS data, we assume that the influence of these is dampened in the long-term median of NO<sub>y</sub>. Both the IAGOS and DC-8 data are gridded to the same 2° latitude × 2.5° longitude grid.

### 2.3 The GEOS-Chem Model

We use the GEOS-Chem global 3D chemical transport model version 13.0.2 (<https://doi.org/10.5281/zenodo.4681204>; last accessed May 2021) to represent contemporary understanding of upper tropospheric NO<sub>y</sub> for comparison to DC-8. The model is driven with consistent MERRA-2 assimilated meteorology at 2° × 2.5° (latitude × longitude) over 47 vertical layers from the surface of the Earth to 0.01 hPa. The model emissions local to the upper troposphere include cruising altitude aircraft from the Aviation Emissions Inventory Code (AEIC) (Stettler et al., 2011) and lightning emissions as described in Murray et al. (2012). Surface emissions of NO<sub>x</sub> and VOCs precursors of ALKNs and PNs are from the anthropogenic Community Emissions Data System (CEDS) inventory of Hoesly et al. (2018), the Model of Emissions of Gases and Aerosols from Nature (MEGAN) biogenic VOCs inventory version 2.1 (Guenther et al., 2012), the soil NO<sub>x</sub> emission inventory of Hudman et al. (2012), and the Global Fire Emissions Database version 4 with small fires (GFED4s) for open burning of biomass (Giglio et al., 2013). Wet deposition of gas-phase HNO<sub>3</sub>, the terminal sink for NO<sub>y</sub> subsiding from the upper troposphere, includes in-cloud (rainout) and below-cloud (washout) scavenging as detailed in Amos et al. (2012) and enhanced scavenging as described by Luo et al. (2020).

We sample the model at the same time and location as the DC-8 observations using the ObsPack diagnostic (<https://www.esrl.noaa.gov/gmd/ccgg/obspack/>; last accessed 23 October 2021) following a minimum 10-month spin-up preceding each campaign to initialize chemistry and large-scale circulation throughout the troposphere.

Modelled components of NO<sub>y</sub> include NO, NO<sub>2</sub>, HNO<sub>3</sub>, HNO<sub>4</sub>, PAN, PPN, peroxyethacroyl nitrate (MPAN), MPN, and ALKNs.

### 3 Results and Discussion

#### 3.1 DC-8 campaign NO<sub>y</sub> seasonality and budget closure

Figure 3 compares seasonality in UT NO<sub>y</sub> from IAGOS and DC-8. Most of the overlap is with ATom along the North Atlantic flight corridor in all seasons, ARCTAS over the Canadian Arctic and Greenland in March-May (MAM) and June-August (JJA), and SEAC<sup>4</sup>RS over the Southeast US in September-November (SON). IAGOS NO<sub>y</sub> exhibits similar peaks in spring (563 pptv) and summer (565 pptv), due to intensive seasonal lightning in the northern hemisphere (Stratmann et al., 2016). Decline in this source decreases NO<sub>y</sub> in autumn to 365 pptv and NO<sub>y</sub> further decreases in winter to an annual minimum of 284 pptv.

DC-8 NO<sub>y</sub> seasonality is similar to that of IAGOS, though the magnitude of DC-8 NO<sub>y</sub> is consistently on average ~130 pptv (range of 80 pptv in SON to 170 pptv in DJF) less than IAGOS NO<sub>y</sub> in all seasons. The ~130 pptv greater IAGOS NO<sub>y</sub> likely results mostly from differences in sampling altitudes. The two campaigns sample distinct altitude ranges of the upper portion of the upper troposphere centred at ~240 hPa (~10 km) for IAGOS and a wider vertical extent of the lower portion of the upper troposphere centred at ~360 hPa (~1.5 km below IAGOS) for DC-8 (Figure S1). There is a general pattern of a steep increase in NO<sub>y</sub> with altitude, with the exception of IAGOS layers located near 300 hPa in March-May and September-November (Figure S1). Average NO<sub>y</sub> is similar between the two campaigns for the rare instances that DC-8 and IAGOS sample the same pressure layers (Figure S1). Another minor factor may be IAGOS NO<sub>y</sub> instrument interference from HCN. The IAGOS chemiluminescence instruments use a hydrogen (H<sub>2</sub>) reagent to convert oxygenated nitrogen compounds to NO, whereas DC-8 uses CO, a compound not permitted on commercial aircraft (Bradshaw et al., 1998; Volz-Thomas et al., 2005; Thomas et al., 2015). The H<sub>2</sub> reagent converts anywhere from 2 to 20% of HCN to NO<sub>y</sub> (Weinheimer, 2006). HCN ambient concentrations typically seasonally vary from ~200 to 300 pptv in the upper troposphere, amounting to an interference of 4-60 pptv (Li et al., 2003; Le Breton et al., 2013).



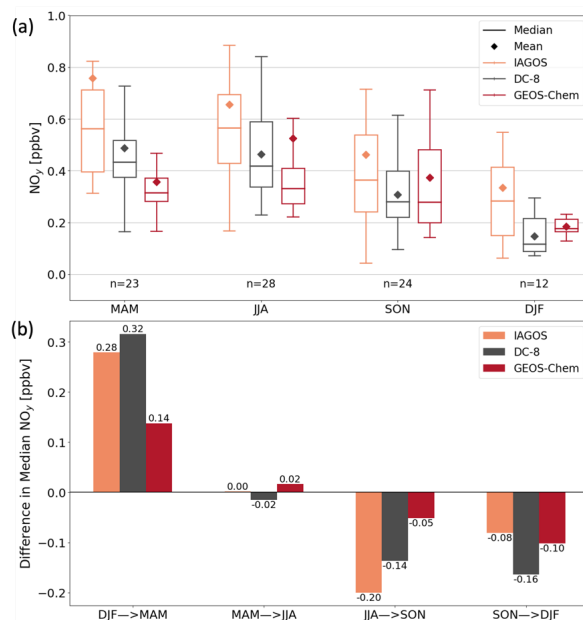


**Figure 3: Seasonality of northern hemisphere upper tropospheric  $\text{NO}_y$ .** Panels show seasonal means and medians (a) and seasonal transitions (b) of collocated gridded  $2^\circ \times 2.5^\circ$   $\text{NO}_y$  from IAGOS (orange), DC-8 (grey), and GEOS-Chem (red). Data in (a) are medians (lines), 25<sup>th</sup> and 75<sup>th</sup> percentiles (boxes) and means (diamonds). Inset text in (a) gives the number (n) of overlapping grid cells. Seasonality in (b) is the change in median  $\text{NO}_y$  in (a) from one season to the next.

Figure 4 shows the relationship between the sum of individual  $\text{NO}_y$  components and total  $\text{NO}_y$  for each DC-8 campaign. We use these scatterplots to determine whether most  $\text{NO}_y$  components are measured in each campaign, given our intention to use DC-8 to assess contemporary understanding of upper tropospheric  $\text{NO}_y$ . The instruments and individual components of  $\text{NO}_y$  summed to compare to total  $\text{NO}_y$  are listed in Table 1. The measured components include  $\text{NO}$ ; PSS  $\text{NO}_2$  (Equation (1));  $\text{HNO}_3$ ; PAN measured as PAN for all ATom sub-campaigns and as part of total PNs for ARCTAS, SEAC<sup>4</sup>RS and KORUS-AQ;  $\text{HNO}_4$  measured as  $\text{HNO}_4$  for ATom-1 and -2 and as part of total PNs for ARCTAS, SEAC<sup>4</sup>RS and KORUS-AQ; C1-C5 ALKNs for all AToms; total ALKNs for SEAC<sup>4</sup>RS, KORUS-AQ, and ARCTAS; PPN and other PANs for all except ATom-1 and -2; and MPN as part of total PNs for ARCTAS, SEAC<sup>4</sup>RS and KORUS-AQ. The evaluation in Figure 4 is biased toward the northern hemisphere, as the low time resolution sampling of the WAS C1-C5 ALKNs during ATom leads to loss of data in the southern hemisphere (Figure 2) to achieve coincidence of DC-8 total and individual components of  $\text{NO}_y$ .

**Table 1.** Observations of individual NO<sub>y</sub> components summed to assess budget closure in Figure 4

| Component        | NASA DC-8 aircraft campaign            |           |           |
|------------------|--|-----------|-----------|
|                  | ARCTAS, SEAC <sup>4</sup> RS, KORUS-AQ | ATom1-2   | ATom3-4   |
| NO <sub>2</sub>  | PSS                                    | PSS       | PSS       |
| NO               | Chemiluminescence (CL)                 | CL        | CL        |
| HNO <sub>3</sub> | CIMS                                   | CIMS      | CIMS      |
| HNO <sub>4</sub> | TD-LIF PNs                             | CIMS      | —         |
| PAN              | TD-LIF PNs                             | PANTHER   | PANTHER   |
| PPN              | TD-LIF PNs                             | —         | CIMS      |
| other PANs       | TD-LIF PNs                             | —         | CIMS      |
| ALKNs            | TD-LIF ALKNs                           | WAS C1-C5 | WAS C1-C5 |
| MPN              | TD-LIF PNs                             | —         | —         |

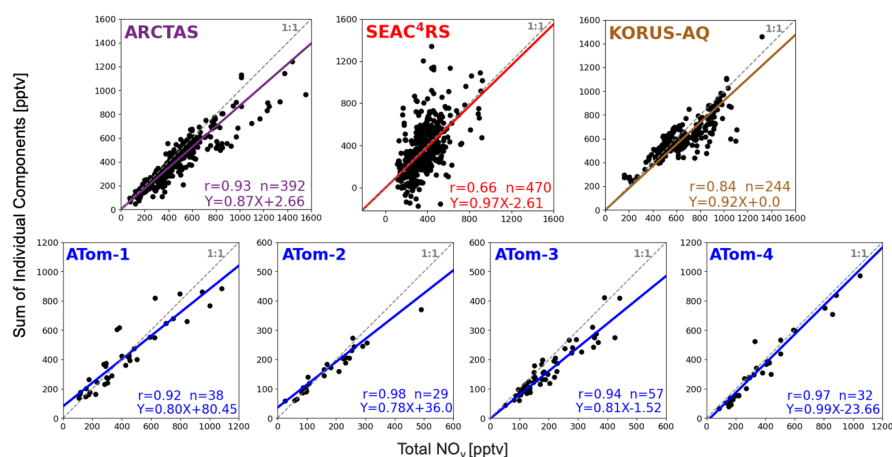


**Figure 4: Proportion of reactive oxidized nitrogen components measured during each campaign. Individual points compare the coincident sum of individual NO<sub>y</sub> components (Table 1) to measured total NO<sub>y</sub> during NASA DC-8 campaigns. Individual NO<sub>y</sub> components used in the figure are detailed in the text. Dashed grey lines are the 1:1 relationship. Coloured lines and inset equations are the Theil-Sen regression fit to the observations. Other inset values are the Pearson's correlation coefficient (r) and number of points (n). Axis ranges differ in each panel.**

Total measured NO<sub>y</sub> and the sum of individual NO<sub>y</sub> components are strongly correlated ( $r > 0.8$ ) for all campaigns, except SEAC<sup>4</sup>RS ( $r = 0.66$ ). The weaker correlation for SEAC<sup>4</sup>RS is from the large contribution of MPN to total PNs measured by the TD-LIF instrument, leading to a large contribution of MPN to total NO<sub>y</sub> for many of the points that stray most from the 1:1 line (Figure S2). If instead we replace TD-LIF PNs with the sum of CIMS PANs and HNO<sub>4</sub>, the correlation with total measured NO<sub>y</sub> increases to  $r = 0.91$ , but the regression slope decreases from 0.97 in Figure 4 to 0.82, as MPN is ~20% of SEAC<sup>4</sup>RS NO<sub>y</sub>. The large contribution of MPN to total NO<sub>y</sub> during SEAC<sup>4</sup>RS (Figure S2) is from aged air initially influenced by lightning, biomass burning and deep convective uplift of surface pollution with large amounts of VOCs and NO<sub>x</sub>. These large amounts of VOCs and NO<sub>x</sub> cause very active photochemistry that enhances abundance of the MPN precursor, CH<sub>3</sub>O<sub>2</sub> (Browne et al., 2011; Nault et al., 2015).

Formatted: Subscript

The regression slopes in Figure 4 indicate that most NO<sub>y</sub> components are measured during each campaign, ranging from 0.78 for ATom-2 (78% of individual NO<sub>y</sub> components measured) to 0.99 for ATom-4 (99% measured). The slopes suggest that between 1-22% of NO<sub>y</sub> originates from factors such as unmeasured components, positive interference in the NO<sub>y</sub> instrument, or low bias in the TD-LIF PNs. Bradshaw et al. (1998) estimated a temperature-dependent interference from HCN of 8-15% for chemiluminescence instruments that, like those deployed on DC-8 campaigns, use a CO reagent. We estimate a lower-end (8%) interference for mean ambient upper troposphere temperatures measured along the flight paths in Figure 2. Using DC-8 HCN observations, this amounts to ~53 ppt or 12% of NO<sub>y</sub> for ARCTAS, ~19 pptv or 5% of NO<sub>y</sub> for SEAC<sup>4</sup>RS, ~40 pptv or 6% NO<sub>y</sub> for KORUS-AQ, and ~17 pptv or 6% NO<sub>y</sub> for ATom 1-4. These lower-end interference estimates are similar in size to the percent unaccounted NO<sub>y</sub> (13% for ARCTAS, 3% for SEAC<sup>4</sup>RS, 8% for KORUS-AQ, 1-22% for ATom).

Chemiluminescence NO<sub>y</sub> instruments also measure pNO<sub>3</sub>, but with uncertain sampling efficiencies (Bourgeois et al., 2022). For 100% sampling efficiency and using the Aerosol Mass Spectrometer (AMS) measurements of submicron (< 1 μm) pNO<sub>3</sub>, we estimate a pNO<sub>3</sub> contribution that is at most 1% of NO<sub>y</sub> for ARCTAS for a median pNO<sub>3</sub> of ~0.01 μg m<sup>-3</sup> (~4 pptv), ~4% for SEAC<sup>4</sup>RS for pNO<sub>3</sub> of ~0.04 μg m<sup>-3</sup> (~14 pptv), ~4% for KORUS-AQ for pNO<sub>3</sub> ~0.07 μg m<sup>-3</sup> (~25 pptv), and <2% for ATom for pNO<sub>3</sub> <0.01 μg m<sup>-3</sup> (~4 pptv).

TD-LIF measurements of PNs are calculated from the difference in NO<sub>2</sub> detected with the NO<sub>2</sub> channel and with the PNs channel set to a temperature at which all PNs decompose (Day et al., 2002). A bias in NO<sub>2</sub> could therefore impart a bias in PNs. The largest source of TD-LIF interference is 100% thermal decomposition of MPN (Reed et al., 2016b) and MPN during SEAC<sup>4</sup>RS far exceeds any of the other campaigns. If we use the higher-end MPN interference of 21% from Shah et al. (2023) for SEAC<sup>4</sup>RS, this equates to ~5 pptv of SEAC<sup>4</sup>RS PSS NO<sub>2</sub>. This is only ~3% of the 190 pptv SEAC<sup>4</sup>RS PNs.

### 3.2 Upper tropospheric NO<sub>y</sub> composition

Figure 5 provides a breakdown of the absolute and relative contributions of individual NO<sub>y</sub> components to total NO<sub>y</sub>. ATom-1 and -4 are combined, as these sub-campaigns have a very similar range in NO<sub>y</sub> (Figure 4) and in median total and individual components of NO<sub>y</sub>, as the sampled seasons (spring and summer) have very similar NO<sub>y</sub> (Figure 3). Similarly, ATom-2 and -3 (autumn and winter) are combined. Campaigns are further grouped into remote (ARCTAS, ATom) and continental (SEAC<sup>4</sup>RS, KORUS-AQ), as local influence from continental sources like anthropogenic emissions and intense lightning leads to a greater relative contribution of NO<sub>x</sub> and lesser contribution of PAN for the continental upper troposphere and vice versa for the remote upper troposphere.

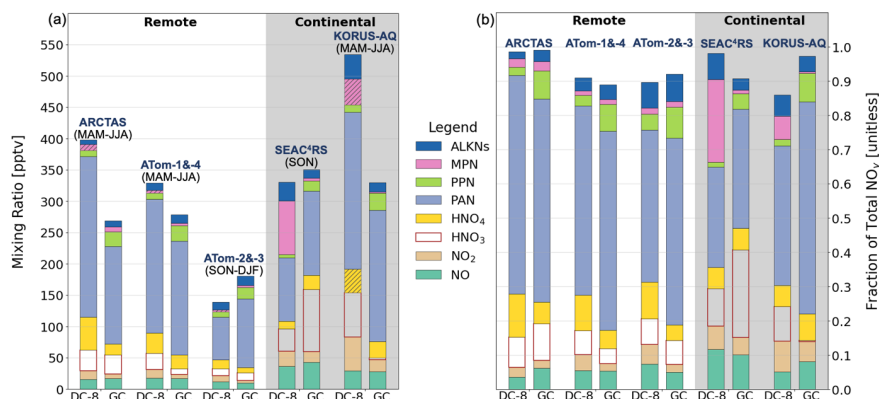


**Figure 5: NO<sub>y</sub> composition in the upper troposphere along DC-8 flight tracks. Bars are median values of absolute (a) and relative (b) individual NO<sub>y</sub> components observed and inferred from the observations during DC-8 campaigns and simulated by GEOS-Chem (GC). Seasons sampled are given above each bar (a) and the grey shading distinguishes sampling in the remote (no shading) and continental (shaded) upper troposphere. Hatching in (a) indicate inferred concentrations (see text for details). Bar components from bottom to top are NO, NO<sub>2</sub>, HNO<sub>3</sub>, HNO<sub>4</sub>, PAN, PPN, MPN, and ALKNs.**

Inferred DC-8 HNO<sub>4</sub> and PPN in Figure 5 use ATom-1 HNO<sub>4</sub> and ATom-4 PPN for combined ATom-1 and -4 components, and, similarly, ATom-2 HNO<sub>4</sub> and ATom-3 PPN for combined ATom-2 and -3. KORUS-AQ HNO<sub>4</sub> is estimated to be 37 pptv by multiplying the SEAC<sup>4</sup>RS median fraction of HNO<sub>4</sub> (HNO<sub>4</sub>/NO<sub>y</sub> = 0.06) by the KORUS-AQ median NO<sub>y</sub>. SEAC<sup>4</sup>RS is used, as HNO<sub>4</sub> is thermally unstable (Ryerson et al., 2000) and so varies with temperature. Mean upper troposphere ambient temperatures for KORUS-AQ (252 K) are more consistent with SEAC<sup>4</sup>RS (246 K) than the other campaigns (238 K for ARCTAS, 238K-241 K for ATom).

The inferred ~10 pptv ARCTAS MPN is from the estimate by Browne et al. (2011). KORUS-AQ MPN is estimated by bounding a potential range from two approaches. The first is the median value of the difference between TD-LIF total PNs and the sum of all individual CIMs PANs and our inferred HNO<sub>4</sub> of 37 pptv, yielding MPN = 75 pptv. This likely overestimates MPN, as the CIMS instrument does not measure an exhaustive suite of PANs. Lee et al. (2022) estimated with a box model and KORUS-AQ measurements that unmeasured PANs account for ~20% of total PNs during KORUS-AQ, though this is for air masses impacted by petrochemical and other anthropogenic VOCs and NO<sub>x</sub> emissions. Accounting for these unmeasured PANs yields a lower-bound KORUS-AQ MPN of 8 pptv. The MPN that we infer then for KORUS-AQ is 42 pptv, the midpoint of 8 and 75 pptv, accounting for 7% of KORUS-AQ NO<sub>y</sub>. As the GEOS-Chem model MPN is consistent with DC-8 inferred MPN during ARCTAS, we multiply the GEOS-Chem ATom MPN fractions (MPN/NO<sub>y</sub> ~0.01 for ATom-1 and -4 and ~0.02 for ATom-2 and -3) by ATom DC-8 NO<sub>y</sub> to infer ATom MPN of < 6 pptv.

Only the C1-C5 ALKNs are shown in Figure 5 for ATom. The remote measurements of total ALKNs available from ARCTAS that would be most suitable to assess the likely contribution of longer chain (>C5) ALKNs are on median 5 pptv less than the ATom C1-C5 ALKNs measurements. The ARCTAS total ALKNs measurements are also very noisy, as indicated by a range of ~113 pptv to ~333 pptv. The range in ARCTAS WAS C1-C5

measurements, by comparison, is 8-29 pptv. Contributions of >C5 ALKNs to total ALKNs for SEAC<sup>4</sup>RS (~50%) and KORUS-AQ (~60%), representative of the continental upper troposphere, suggest that >C5 ALKNs in remote regions are <50% of total ALKNs or <12 pptv (median of C1-C5 ALKNs for ATom1-4). According to the measurements, remote region C1-C5 ALKNs are dominated by methyl nitrate (C1 ALKN), accounting for 40% of ATom C1-C5 ALKNs and 49% for ARCTAS. Second is isopropyl nitrate (C3 ALKN), making up 17% of ATom C1-C5 ALKNs and 25% for ARCTAS. The >C3 ALKNs dominate ALKNs in the continental upper troposphere, accounting for 92% of total ALKNs for SEAC<sup>4</sup>RS and 71% for KORUS-AQ. These we estimate as the difference between TD-LIF total ALKNs and the sum of WAS C1-C3 ALKNs.

The sum of KORUS-AQ NO<sub>y</sub> components total 531 pptv, >130 pptv more than SEAC<sup>4</sup>RS, ARCTAS, and ATom-1 and -4 that are within a narrow range of 330-400 pptv. Minimum NO<sub>y</sub> are for the remote autumn and winter measurements from ATom-2 and -3 at 141 pptv. Despite the wide range in absolute total and components of NO<sub>y</sub>, the relative contribution of many individual NO<sub>y</sub> components is consistent across all campaigns. These include NO (7 ± 3%; mean ± 1σ standard deviation), NO<sub>2</sub> (6 ± 2%), HNO<sub>3</sub> (9 ± 2%), HNO<sub>4</sub> (9 ± 3%), PPN (3 ± 1%), and ALKNs (5 ± 3%). PAN, the dominant NO<sub>y</sub> component in all campaigns, is least consistent, ranging from 30-41% for the continental upper troposphere to 44-64% for the remote upper troposphere. The HNO<sub>4</sub> fraction (10-13%) in the remote upper troposphere is more than the continental upper troposphere (~6%), due to colder temperatures for ATom and ARCTAS. MPN is uniquely prominent during SEAC<sup>4</sup>RS, accounting for 24% of NO<sub>y</sub> compared to 2-7% inferred for all other campaigns. pNO<sub>3</sub>, absent in Figure 5 due to the uncertain sampling efficiency of the chemiluminescence instrument, is at most 4% for SEAC<sup>4</sup>RS and KORUS-AQ (Section 3.1), comparable to the contribution from PPN.

The far larger fraction of MPN to total NO<sub>y</sub> during SEAC<sup>4</sup>RS (Figure 5(b)) warrants further investigation, as the relative proportion of MPN to total NO<sub>y</sub> ranges from negligible to 100% (Figure S2). If we instead estimate MPN by subtracting the sum of HNO<sub>4</sub> and all PANs measured with the CIMS instrument from the TD-LIF PNs, making the assumption that CIMS measures most PANs, MPN is 49 pptv and the SEAC<sup>4</sup>RS median contribution to NO<sub>y</sub> declines from 24% to 14%. This is still at least double the contribution for any other campaign. A small proportion of HNO<sub>4</sub> is measured in the MPN channel of the TD-LIF instrument. About 11%, according to Nault et al. (2015). For CIMS median HNO<sub>4</sub> of 12.6 pptv during SEAC<sup>4</sup>RS, HNO<sub>4</sub> interference is only 1.4 pptv, so does not affect the 14-24% contribution.

The NO<sub>y</sub> composition information in Figure 5 has a northern hemisphere sampling bias to achieve coincidence. ATom observations south of the Equator exhibit a similar seasonal pattern to the northern hemisphere: summer > spring > autumn > winter NO<sub>y</sub>, except that the southern hemisphere spring and summer NO<sub>y</sub> differ by ~90 pptv, whereas there is near-negligible difference for the northern hemisphere (Figure 3). As with the northern hemisphere, PAN accounts for most southern hemisphere NO<sub>y</sub>, ranging from ~32% for ATom-1 (July-August) to ~42% for ATom-2 (January-February).

Nighttime dominant NO<sub>y</sub> compounds N<sub>2</sub>O<sub>5</sub>, NO<sub>3</sub>, and HONO are not included in Figure 5, as these have near-negligible daytime abundances. Of these, there are only measurements of N<sub>2</sub>O<sub>5</sub>, limited to ATom-3 and -4, that

Formatted: Subscript

Formatted: Subscript

Formatted: Superscript

Formatted: Subscript

represent ~0.1% of upper tropospheric NO<sub>y</sub> along the daytime ATom flight tracks in Figure 2. NO<sub>3</sub> has a lifetime of a few seconds during the day, due to efficient photolysis (Brown and Stutz, 2012). HONO also rapidly photolyzes with a near-surface lifetime of 15 min (Sörgel et al., 2011). Photolysis of HONO would be further enhanced (by ~50% at 390 nm) in the upper troposphere where photolysis frequencies are enhanced (Hofzumahaus et al., 2002; Reed et al., 2016a).

### 3.3 Contemporary understanding of UT NO<sub>y</sub>

GEOS-Chem northern hemisphere upper troposphere NO<sub>y</sub> is compared to the observations in Figures 3 and 5. In Figure 3, GEOS-Chem median NO<sub>y</sub> is less than DC-8 in summer and spring by ~103 pptv, similar to DC-8 in autumn, and greater than DC-8 in winter by ~60 pptv. As a result of these differences in absolute NO<sub>y</sub>, the model underestimates the IAGOS and DC-8 seasonal shifts in NO<sub>y</sub> from winter to spring and from summer to autumn.

The sum of the GEOS-Chem fractional contributions of NO<sub>y</sub> components in Figure 5(b) that do not sum to 1 are because the model NO<sub>y</sub> budget also includes components not measured during DC-8, such as MPAN and halogenated ALKNs. Consistent across all campaigns is model underestimate in NO<sub>2</sub> and overestimate in PPN. The model version we use does not include photolysis of PPN, even though this is known to occur (Harwood et al., 2003). PPN photolysis rather than thermal decomposition is the dominant loss pathway of PPN in the cold upper troposphere. PPN photolysis is scheduled for inclusion in a later model version (version 14.5) than is used here (Horner et al., 2024). Inclusion of PPN photolysis would liberate up to ~16 pptv NO<sub>2</sub>, resolving the 10-16 pptv model underestimate in NO<sub>2</sub>. Other studies have addressed model biases in NO<sub>2</sub> by including photolysis of pNO<sub>3</sub> forming HONO that rapidly photolyzes to NO<sub>x</sub> (Shah et al., 2023; Horner et al., 2024). pNO<sub>3</sub> concentrations are too small in the upper troposphere for this to be a substantial NO<sub>2</sub> source. These are on median, ~0.01 µg m<sup>-3</sup> during ARCTAS, ~0.07 µg m<sup>-3</sup> during KORUS-AQ, ~0.04 µg m<sup>-3</sup> during SEAC<sup>4</sup>RS and <0.01 µg m<sup>-3</sup> during ATom (Section 3.1).

The model exhibits significant campaign-specific biases in total NO<sub>y</sub> for ARCTAS (129 pptv underestimate), KORUS-AQ (205 pptv underestimate), ATom-1 and -4 (51 pptv underestimate) and ATom-2 and -3 (42 pptv overestimate). The model underestimate in ARCTAS NO<sub>y</sub> is due mostly to a ~100 pptv low bias in PAN and, to a lesser extent, a 35 pptv underestimate in HNO<sub>4</sub>. The model bias for ATom-2 and -3 is due almost entirely to PAN. For KORUS-AQ, all NO<sub>y</sub> components except PPN are underestimated, indicative of an overall underestimate in NO<sub>y</sub> sources to the upper troposphere over this region. The ATom-1 and -4 underestimate in NO<sub>y</sub> is due mostly to a low model bias in PAN and HNO<sub>3</sub>. Overall, the model underestimates the contrast in upper tropospheric NO<sub>y</sub> between the remote and continental upper troposphere.

GEOS-Chem simulates individual C1-C3 ALKNs, but most >C3 ALKNs are included as a lumped species. There are other >C3 ALKNs represented individually in the model, such as those formed from isoprene oxidation (Fisher et al., 2016), but abundances of these are near-negligible in the upper troposphere. DC-8 C1 ALKN is only 4% of ALKNs for SEAC<sup>4</sup>RS and 11% for KORUS-AQ, whereas in the model these are a much greater component of ALKNs: 40% for SEAC<sup>4</sup>RS and 29% for KORUS-AQ. Modelled >C3 ALKNs are a far smaller portion of total

ALKNs (29% for SEAC<sup>4</sup>RS and 23% for KORUS-AQ) than the observations (Sect. 3.2). Modelled C1 ALKN concentrations are consistently less than the observed values by ~2 pptv for ARCTAS and ~1 pptv for ATom. Modelled C3 ALKN is ~1 pptv less than the observations for ARCTAS, but ~1 pptv more than the observations for ATom.

The sum of measured and modelled individual NO<sub>y</sub> components are not significantly different for SEAC<sup>4</sup>RS, though the model overestimates HNO<sub>3</sub> by 64 pptv and underestimates MPN by 81 pptv compared to the TD-LIF measurements and by 45 pptv compared to MPN inferred using TD-LIF PNs and CIMS HNO<sub>4</sub> and PANs (Section 3.2). The model low bias in MPN suggests that the model underestimates influence of NO<sub>x</sub> and reactive VOCs sources on aged air over source regions with a mix of emissions from fires and lightning, and deep convective injection of surface pollution. Chen et al. (2019) estimated that the GEOS-Chem underestimate in free tropospheric VOCs during SEAC<sup>4</sup>RS is on average ~60%, but exceeds a factor of 2 for many of the VOCs assessed. The model high bias in HNO<sub>3</sub> could be because of a factor of 2 overestimate in our modelled H<sub>2</sub>O<sub>2</sub> compared to observed H<sub>2</sub>O<sub>2</sub> for SEAC<sup>4</sup>RS. An overestimate in H<sub>2</sub>O<sub>2</sub> indicates a model overestimate in HO<sub>2</sub> that promotes formation of HNO<sub>3</sub> and that would also account for the ~10 pptv overestimate in modelled HNO<sub>4</sub>. Modelled HO<sub>2</sub> is used to calculate PSS NO<sub>2</sub> for SEAC<sup>4</sup>RS (Equation (1), Sect. 2.1), but this only imparts a small high bias (~1.7 pptv) in SEAC<sup>4</sup>RS PSS NO<sub>2</sub>. Model bias in H<sub>2</sub>O<sub>2</sub> for ARCTAS (>100 pptv) may also be the cause for the model underestimate in ARCTAS HNO<sub>4</sub> of ~35 pptv.

Modelled KORUS-AQ HNO<sub>3</sub>, ALKNs, and MPN are all biased low. The low biases in these NO<sub>y</sub> components may be because of a general underestimate in NO<sub>y</sub> sources over South Korea where there are large anthropogenic NO<sub>x</sub> and VOCs sources that are represented in the model with a global inventory (CEDs) that may not suitably account for local emissions (Travis et al., 2024). Lightning NO<sub>x</sub> emissions could also be underestimated in the heavily parameterized inventory in GEOS-Chem (Murray et al., 2012; Marais et al., 2018), but this is a challenging NO<sub>x</sub> source to evaluate over locations that include other prominent sources of NO<sub>x</sub>.

The model biases identified in this work hinder accurate determination of the radiative effect of tropospheric ozone for short-term climate impact assessments, the oxidative capacity of the troposphere for quantifying the lifetime and persistence of the greenhouse gas methane, tropospheric column densities of NO<sub>2</sub> from space-based UV-visible instruments that are retrieved with modelled vertical profiles of NO<sub>2</sub>, NO<sub>x</sub> emissions by comparing modelled and observed oxidized nitrate wet deposition fluxes that depend on the abundance of soluble HNO<sub>3</sub>, and harm of nitrogen deposition to vulnerable habitats.

#### 4 Conclusions

We used NASA DC-8 aircraft measurement data from the ARCTAS, SEAC<sup>4</sup>RS, KORUS-AQ, and ATom campaigns to characterize reactive oxidized nitrogen (NO<sub>y</sub>) in the global upper troposphere. This followed confirmation from comparison to routine total NO<sub>y</sub> measurements from the IAGOS commercial aircraft campaign that DC-8 has the same seasonality of peak NO<sub>y</sub> in summer and spring and minimum NO<sub>y</sub> in winter in the northern

hemisphere. Consistency supports use of DC-8 campaign data to characterise NO<sub>y</sub> under standard daytime conditions.

We also confirm that most (78-99%) NO<sub>y</sub> components were measured during DC-8 campaigns. These include nitrogen oxides (NO<sub>x</sub>), and inorganic (HNO<sub>3</sub> and HNO<sub>4</sub>), and organic (PANs, MPN, and alkyl nitrates) reservoirs of NO<sub>x</sub>. PAN is the dominant NO<sub>y</sub> component for all campaigns (30-64%), followed by NO<sub>x</sub> (6-18%), HNO<sub>4</sub> (6-13%) and HNO<sub>3</sub> (7-11%). The relative contribution of most other components is similar across all campaigns, except for MPN that is 14-24% of NO<sub>y</sub> for SEAC<sup>4</sup>RS over the Southeast US and much less (2-7%) for all other campaigns, though MPN measurements are rare and susceptible to biases.

The GEOS-Chem model is sampled along the DC-8 flight tracks to assess the state of knowledge of upper tropospheric NO<sub>y</sub>. Consistent model biases for all campaigns include an overestimate in PPN and underestimate in NO<sub>2</sub>. The model lacks PPN photolysis that would address the PPN model bias and mostly resolve the NO<sub>2</sub> bias. In the continental upper troposphere, the model underestimates total NO<sub>y</sub> for KORUS-AQ, but reproduces total NO<sub>y</sub> for SEAC<sup>4</sup>RS, though with too much HNO<sub>3</sub> and too little MPN. Over remote regions, the model biases are less severe, and are likely related to the weak seasonal variability in total NO<sub>y</sub> in comparison to DC-8 and IAGOS. A possible cause of this is errors in model representation of maritime lightning NO<sub>x</sub> emissions that influence NO<sub>y</sub> abundance in spring and summer.

Our results underscore the need for sustained measurements of upper tropospheric reactive oxidized nitrogen for further refinement of knowledge of upper tropospheric NO<sub>y</sub> sources, advection, and chemical processing. This is crucial for advancing our understanding of the global nitrogen cycle and its broader environmental impacts.

#### Author Contributions

Study concept by EAM and NW. NW led the data analysis and simulated GEOS-Chem. The manuscript is initiated by NW and co-written by EAM. GL aided in data analysis, RGR in the use of ObsPack, and BS in the use of IAGOS NO<sub>y</sub> observations. All authors reviewed and edited the manuscript.

#### Competing interests

The authors declare that they have no conflict of interest.

#### Acknowledgements

We are grateful for the provision of the NASA DC-8 aircraft observations by the instrument PIs Paul O. Wennberg, Ronald C. Cohen, Thomas B. Ryerson, Chelsea Thompson, Andrew Weinheimer, L. Gregory Huey, Jim Elkins, and Donald R. Blake and, for IAGOS, the IAGOS-Core data provided by Andreas Volz-Thomas and IAGOS-CARABIC by Helmut Ziereis. The authors acknowledge the strong support of the European Commission, Airbus, and the airlines (Lufthansa, Air France, Austrian Airlines, Air Namibia, Cathay Pacific, Iberia and China Airlines so far) who have carried the IAGOS-Core equipment and performed the maintenance since 1994. IAGOS-CARABIC NO<sub>y</sub> measurement funding is from the German Aerospace Centre (DLR). In its last 10 years of operation, IAGOS-Core has been funded by INSU-CNRS (France), Météo-France, Université Paul Sabatier



(Toulouse, France) and Forschungszentrum Jülich (FZJ, Jülich, Germany). IAGOS has been additionally funded by the EU projects IAGOSDS and IAGOS-ERI. The IAGOS-Core and the IAGOS-CARIBIC database are supported by AERIS. IAGOS-CARIBIC data are also available from the IAGOS-CARIBIC team (see <http://www.caribic-atmospheric.com> )

#### Data and Software Availability

All data and software used in this study are from publicly accessible repositories: Zenodo for GEOS-Chem (The International GEOS-Chem User Community, 2021), the AERIS data service for IAGOS (Boulanger et al., 2018), and NASA data archives for ARCTAS (NASA, 2009), SEAC<sup>4</sup>RS (NASA, 2015), KORUS-AQ (NASA, 2017), and ATom (NASA, 2021).

#### Funding

This research has been supported by the European Research Council under the European Union's Horizon 2020 research and innovation programme (through a Starting Grant awarded to Eloise A. Marais, UpTrop [grant no. 851854]).

#### References

- Amos, H. M., Jacob, D. J., Holmes, C., Fisher, J. A., Wang, Q., Yantosca, R. M., Corbitt, E. S., Galarneau, E., Rutter, A., and Gustin, M.: Gas-particle partitioning of atmospheric Hg (II) and its effect on global mercury deposition, *Atmos. Chem. Phys.*, 12, 591-603, doi:10.5194/acp-12-591-2012, 2012.
- Barth, M. C., Cantrell, C. A., Brune, W. H., Rutledge, S. A., Crawford, J. H., Huntrieser, H., Carey, L. D., MacGorman, D., Weisman, M., Pickering, K. E., et al.: The Deep Convective Clouds and Chemistry (DC3) Field Campaign, *B. Am. Meteorol. Soc.*, 96, 1281-1309, doi:10.1175/bams-d-13-00290.1, 2015.
- Bertram, T. H., Perring, A. E., Wooldridge, P. J., Crounse, J. D., Kwan, A. J., Wennberg, P. O., Scheuer, E., Dibb, J., Avery, M., Sachse, G., et al.: Direct measurements of the convective recycling of the upper troposphere, *Science*, 315, 816-820, doi:10.1126/science.1134548, 2007.
- Blake, N. J., Blake, D. R., Swanson, A. L., Atlas, E., Flocke, F., and Rowland, F. S.: Latitudinal, vertical, and seasonal variations of C1-C4 alkyl nitrates in the troposphere over the Pacific Ocean during PEM-Tropics A and B: Oceanic and continental sources, *J. Geophys. Res.-Atmos.*, 108, doi:10.1029/2001JD001444, 2003.
- Blakeslee, R. J., Mach, D. M., Bateman, M. G., and Bailey, J. C.: Seasonal variations in the lightning diurnal cycle and implications for the global electric circuit, *Atmos. Res.*, 135-136, 228-243, doi:10.1016/j.atmosres.2012.09.023, 2014.
- Boersma, K. F., Eskes, H. J., Dirksen, R. J., van der A, R. J., Veefkind, J. P., Stammes, P., Huijnen, V., Kleipool, Q. L., Sneep, M., Claas, J., et al.: An improved tropospheric NO<sub>2</sub> column retrieval algorithm for the Ozone Monitoring Instrument, *Atmos. Meas. Tech.*, 4, 1905-1928, doi:10.5194/amt-4-1905-2011, 2011.
- Boulanger, D., Blot, R., Bundke, U., Gerbig, C., Hermann, M., Nédélec, P., Rohs, S., and Ziereis, H.: IAGOS final quality controlled Observational Data L2 – Vertical profiles. [dataset]. AERIS, [last accessed: 3 September 2021], 2018.
- Bourgeois, I., Peischl, J., Neuman, J. A., Brown, S. S., Allen, H. M., Campuzano-Jost, P., Coggon, M. M., DiGangi, J. P., Diskin, G. S., Gilman, J. B., et al.: Comparison of airborne measurements of NO, NO<sub>2</sub>, HONO, NO<sub>y</sub>, and CO during FIREX-AQ, *Atmos. Meas. Tech.*, 15, 4901-4930, doi:10.5194/amt-15-4901-2022, 2022.

- Bradshaw, J., Sandholm, S., and Talbot, R.: An update on reactive odd-nitrogen measurements made during recent NASA Global Tropospheric Experiment programs, *J. Geophys. Res.-Atmos.*, 103, 19129-19148, doi:10.1029/98JD00621, 1998.
- 580 Bradshaw, J., Davis, D., Grodzinsky, G., Smyth, S., Newell, R., Sandholm, S., and Liu, S.: Observed distributions of nitrogen oxides in the remote free troposphere from the NASA Global Tropospheric Experiment Programs, *Rev. Geophys.*, 38, 61-116, doi:10.1029/1999rg900015, 2000.
- Brasseur, G. P., Müller, J.-F., and Granier, C.: Atmospheric impact of NO<sub>x</sub> emissions by subsonic aircraft: A three dimensional model study, *J. Geophys. Res.-Atmos.*, 101, 1423-1428, doi:10.1029/95jd02363, 1996.
- 585 Brenninkmeijer, C. A. M., Crutzen, P., Boumard, F., Dauer, T., Dix, B., Ebinghaus, R., Filippi, D., Fischer, H., Franke, H., Friß, U., et al.: Civil aircraft for the regular investigation of the atmosphere based on an instrumented container: The new CARIBIC system, *Atmos. Chem. Phys.*, 7, 4953-4976, doi:10.5194/acp-7-4953-2007, 2007.
- Brown, S. S., and Stutz, J.: Nighttime radical observations and chemistry, *Chem. Soc. Rev.*, 41, 6405-6447, doi:10.1039/C2CS35181A, 2012.
- 590 Browne, E. C., Perring, A. E., Wooldridge, P. J., Apel, E., Hall, S. R., Huey, L. G., Mao, J., Spencer, K. M., Clair, J. M. S., Weinheimer, A. J., et al.: Global and regional effects of the photochemistry of CH<sub>3</sub>O<sub>2</sub>NO<sub>2</sub>: Evidence from ARCTAS, *Atmos. Chem. Phys.*, 11, 4209-4219, doi:10.5194/acp-11-4209-2011, 2011.
- Burkholder, J. B., Sander, S. P., Abbatt, J., Barker, J. R., Cappa, C., Crounse, J. D., Dibble, T. S., Huie, R. E., Kolb, C. E., Kurylo, M. J., Orkin, V. L., Percival, C. J., Wilmouth, D. M., and Wine, P. H.: Chemical kinetics and photochemical data for use in atmospheric studies, evaluation No. 19, JPL Publication 19-5, 2020.
- 595 Chen, X., Millet, D. B., Singh, H. B., Wisthaler, A., Apel, E. C., Atlas, E. L., Blake, D. R., Bourgeois, I., Brown, S. S., Crounse, J. D., et al.: On the sources and sinks of atmospheric VOCs: An integrated analysis of recent aircraft campaigns over North America, *Atmos. Chem. Phys.*, 19, 9097-9123, doi:10.5194/acp-19-9097-2019, 2019.
- 600 Cohen, Y., Hauglustaine, D., Sauvage, B., Rohs, S., Konjari, P., Bundke, U., Petzold, A., Thouret, V., Zahn, A., and Ziereis, H.: Evaluation of modelled climatologies of O<sub>3</sub>, CO, water vapour and NO<sub>y</sub> in the upper troposphere–lower stratosphere using regular in situ observations by passenger aircraft, *Atmos. Chem. Phys.*, 23, 14973-15009, doi:10.5194/acp-23-14973-2023, 2023.
- 605 Crawford, J. H., Ahn, J.-Y., Al-Saadi, J., Chang, L., Emmons, L. K., Kim, J., Lee, G., Park, J.-H., Park, R. J., Woo, J. H., et al.: The Korea–United States Air Quality (KORUS-AQ) field study, *Elementa: Science of the Anthropocene*, 9, doi:10.1525/elementa.2020.00163, 2021.
- Crounse, J. D., McKinney, K. A., Kwan, A. J., and Wennberg, P. O.: Measurement of gas-phase hydroperoxides by Chemical Ionization Mass Spectrometry, *Anal. Chem.*, 78, 6726-6732, doi:10.1021/ac0604235, 2006.
- 610 Culter, F., NASA DC-8 Flying Laboratory Aircraft, [https://ghrc.nsstc.nasa.gov/home/sites/default/files/cutler\\_dc8.pdf](https://ghrc.nsstc.nasa.gov/home/sites/default/files/cutler_dc8.pdf), [last accessed: 3 October 2024], 2009.
- Dahlmann, K., Grewe, V., Ponater, M., and Matthes, S.: Quantifying the contributions of individual NO<sub>x</sub> sources to the trend in ozone radiative forcing, *Atmos. Environ.*, 45, 2860-2868, doi:10.1016/j.atmosenv.2011.02.071, 2011.

- 615 Dameris, M.: Stratosphere/Troposphere exchange and structure | Tropopause, in: Encyclopedia of Atmospheric Sciences (Second Edition), edited by: North, G. R., Pyle, J., and Zhang, F., Academic Press, Oxford, 269-272, doi:<https://doi.org/10.1016/B978-0-12-382225-3.00418-7>, 2015.
- Day, D. A., Wooldridge, P. J., Dillon, M. B., Thornton, J. A., and Cohen, R. C.: A thermal dissociation laser-induced fluorescence instrument for in situ detection of NO<sub>2</sub>, peroxy nitrates, alkyl nitrates, and HNO<sub>3</sub>, *J. Geophys. Res.: Atmos.*, 107, doi:10.1029/2001jd000779, 2002.
- 620 Ehhalt, D. H., Rohrer, F., and Wahner, A.: Sources and distribution of NO<sub>x</sub> in the upper troposphere at northern mid-latitudes, *J. Geophys. Res.-Atmos.*, 97, 3725-3738, doi:10.1029/91JD03081, 1992.
- Emmons, L. K., Carroll, M. A., Hauglustaine, D. A., Brasseur, G. P., Atherton, C., Penner, J., Sillman, S., Levy, H., Rohrer, F., Wauben, W. M. F., et al.: Climatologies of NO<sub>x</sub> and NO<sub>y</sub>: A comparison of data and models, *Atmos. Environ.*, 31, 1851-1904, doi:10.1016/s1352-2310(96)00334-2, 1997.
- 625 Fisher, J. A., Jacob, D. J., Travis, K. R., Kim, P. S., Marais, E. A., Chan Miller, C., Yu, K., Zhu, L., Yantosca, R. M., Sulprizio, M. P., et al.: Organic nitrate chemistry and its implications for nitrogen budgets in an isoprene- and monoterpene-rich atmosphere: constraints from aircraft (SEAC<sup>4</sup>RS) and ground-based (SOAS) observations in the Southeast US, *Atmos. Chem. Phys.*, 16, 5969-5991, doi:10.5194/acp-16-5969-2016, 2016.
- 630 Fisher, J. A., Atlas, E. L., Barletta, B., Meinardi, S., Blake, D. R., Thompson, C. R., Ryerson, T. B., Peischl, J., Tzompa-Sosa, Z. A., and Murray, L. T.: Methyl, ethyl, and propyl nitrates: Global distribution and impacts on reactive nitrogen in remote marine environments, *J. Geophys. Res.-Atmos.*, 123, doi:10.1029/2018jd029046, 2018.
- Fuelberg, H. E., Hannan, J. R., van Velthoven, P. F. J., Browell, E. V., Bieberbach Jr., G., Knabb, R. D., Gregory, G. L., Pickering, K. E., and Selkirk, H. B.: A meteorological overview of the Subsonic Assessment Ozone and Nitrogen Oxide Experiment (SONEX) period, *J. Geophys. Res.-Atmos.*, 105, 3633-3651, doi:10.1029/1999JD900917, 2000.
- 635 Giglio, L., Randerson, J. T., and van der Werf, G. R.: Analysis of daily, monthly, and annual burned area using the fourth-generation global fire emissions database (GFED4), *J. Geophys. Res.-Biogeo.*, 118, 317-328, doi:10.1002/jgrg.20042, 2013.
- 640 Gressent, A., Sauvage, B., Defer, E., Pätz, H. W., Thomas, K., Holle, R., Cammas, J.-P., Nédélec, P., Boulanger, D., Thouret, V., et al.: Lightning NO<sub>x</sub> influence on large-scale NO<sub>y</sub> and O<sub>3</sub> plumes observed over the northern mid-latitudes, *Tellus B*, 66, doi:10.3402/tellusb.v66.25544, 2014.
- Gressent, A., Sauvage, B., Cariolle, D., Evans, M., Leriche, M., Mari, C., and Thouret, V.: Modeling lightning-NO<sub>x</sub> chemistry on a sub-grid scale in a global chemical transport model, *Atmos. Chem. Phys.*, 16, 5867-5889, doi:10.5194/acp-16-5867-2016, 2016.
- 645 Guenther, A. B., Jiang, X., Heald, C. L., Sakulyanontvittaya, T., Duhl, T., Emmons, L. K., and Wang, X.: The Model of Emissions of Gases and Aerosols from Nature version 2.1 (MEGAN2.1): An extended and updated framework for modeling biogenic emissions, *Geosci. Model Dev.*, 5, 1471-1492, doi:10.5194/gmd-5-1471-2012, 2012.
- 650 Harwood, M. H., Roberts, J. M., Frost, G. J., Ravishankara, A. R., and Burkholder, J. B.: Photochemical Studies of CH<sub>3</sub>C(O)OONO<sub>2</sub> (PAN) and CH<sub>3</sub>CH<sub>2</sub>C(O)OONO<sub>2</sub> (PPN): NO<sub>3</sub> Quantum Yields, *J. Phys. Chem. A*, 107, 1148-1154, doi:10.1021/jp0264230, 2003.
- Hoesly, R. M., Smith, S. J., Feng, L., Klimont, Z., Janssens-Maenhout, G., Pitkanen, T., Seibert, J. J., Vu, L., Andres, R. J., Bolt, R. M., et al.: Historical (1750–2014) anthropogenic emissions of reactive gases and aerosols
- 655

- from the Community Emissions Data System (CEDS), *Geosci. Model Dev.*, 11, 369-408, doi:10.5194/gmd-11-369-2018, 2018.
- 660 Hofzumahaus, A., Kraus, A., Kylling, A., and Zerefos, C. S.: Solar actinic radiation (280–420 nm) in the cloud-free troposphere between ground and 12 km altitude: Measurements and model results, *J. Geophys. Res.-Atmos.*, 107, doi:10.1029/2001jd900142, 2002.
- Horner, R. P., Marais, E. A., Wei, N., Ryan, R. G., and Shah, V.: Vertical profiles of global tropospheric nitrogen dioxide (NO<sub>2</sub>) obtained by cloud slicing the TROPOspheric Monitoring Instrument (TROPOMI), *Atmos. Chem. Phys.*, 24, 13047-13064, doi:10.5194/acp-24-13047-2024, 2024.
- 665 Hudman, R. C., Jacob, D. J., Turquety, S., Leibensperger, E. M., Murray, L. T., Wu, S., Gilliland, A. B., Avery, M., Bertram, T. H., Brune, W., et al.: Surface and lightning sources of nitrogen oxides over the United States: Magnitudes, chemical evolution, and outflow, *J. Geophys. Res.*, 112, doi:10.1029/2006jd007912, 2007.
- Hudman, R. C., Moore, N. E., Mebust, A. K., Martin, R. V., Russell, A. R., Valin, L. C., and Cohen, R. C.: Steps towards a mechanistic model of global soil nitric oxide emissions: implementation and space based-constraints, *Atmos. Chem. Phys.*, 12, 7779-7795, doi:10.5194/acp-12-7779-2012, 2012.
- 670 Huey, L. G.: Measurement of trace atmospheric species by chemical ionization mass spectrometry: Speciation of reactive nitrogen and future directions, *Mass Spectrom. Rev.*, 26, 166-184, doi:10.1002/mas.20118, 2007.
- Huntrieser, H., Lichtenstern, M., Scheibe, M., Aufmhoff, H., Schlager, H., Pucik, T., Minikin, A., Weinzierl, B., Heimerl, K., Pollack, I. B., et al.: Injection of lightning-produced NO<sub>x</sub>, water vapor, wildfire emissions, and stratospheric air to the UT/LS as observed from DC3 measurements, *J. Geophys. Res.-Atmos.*, 121, 6638-6668, doi:10.1002/2015JD024273, 2016.
- 675 Jacob, D. J., Crawford, J. H., Maring, H., Clarke, A. D., Dibb, J. E., Emmons, L. K., Ferrare, R. A., Hostetler, C. A., Russell, P. B., Singh, H. B., et al.: The Arctic Research of the Composition of the Troposphere from Aircraft and Satellites (ARCTAS) mission: Design, execution, and first results, *Atmos. Chem. Phys.*, 10, 5191-5212, doi:10.5194/acp-10-5191-2010, 2010.
- 680 Jaeglé, L., Jacob, D. J., Wang, Y., Weinheimer, A. J., Ridley, B. A., Campos, T. L., Sachse, G. W., and Hagen, D. E.: Sources and chemistry of NO<sub>x</sub> in the upper troposphere over the United States, *Geophys. Res. Lett.*, 25, 1705-1708, doi:10.1029/97gl03591, 1998.
- Le Breton, M., Bacak, A., Muller, J. B. A., O'Shea, S. J., Xiao, P., Ashfold, M. N. R., Cooke, M. C., Batt, R., Shallcross, D. E., Oram, D. E., et al.: Airborne hydrogen cyanide measurements using a chemical ionisation mass spectrometer for the plume identification of biomass burning forest fires, *Atmos. Chem. Phys.*, 13, 9217-9232, doi:10.5194/acp-13-9217-2013, 2013.
- 685 Lee, Y. R., Huey, L. G., Tanner, D. J., Takeuchi, M., Qu, H., Liu, X., Ng, N. L., Crawford, J. H., Fried, A., Richter, D., et al.: An investigation of petrochemical emissions during KORUS-AQ: Ozone production, reactive nitrogen evolution, and aerosol production, *Elementa: Science of the Anthropocene*, 10, doi:10.1525/elementa.2022.00079, 2022.
- 690 Levy II, H., Mahlman, J. D., and Moxim, W. J.: A stratospheric source of reactive nitrogen in the unpolluted troposphere, *Geophys. Res. Lett.*, 7, 441-444, doi:10.1029/GL007i006p00441, 1980.
- Levy II, H., Moxim, W. J., Klonecki, A. A., and Kasibhatla, P. S.: Simulated tropospheric NO<sub>x</sub>: Its evaluation, global distribution and individual source contributions, *J. Geophys Res.-Atmos.*, 104, 26279-26306, doi:10.1029/1999JD900442, 1999.
- 695

- Li, Q., Jacob, D. J., Yantosca, R. M., Heald, C. L., Singh, H. B., Koike, M., Zhao, Y., Sachse, G. W., and Streets, D. G.: A global three-dimensional model analysis of the atmospheric budgets of HCN and CH<sub>3</sub>CN: Constraints from aircraft and ground measurements, *J. Geophys. Res.-Atmos.*, 108, doi:10.1029/2002JD003075, 2003.
- 700 Liang, Q., Rodriguez, J. M., Douglass, A. R., Crawford, J. H., Olson, J. R., Apel, E., Bian, H., Blake, D. R., Brune, W., Chin, M., et al.: Reactive nitrogen, ozone and ozone production in the Arctic troposphere and the impact of stratosphere-troposphere exchange, *Atmos. Chem. Phys.*, 11, 13181-13199, doi:10.5194/acp-11-13181-2011, 2011.
- 705 Logan, J. A.: Nitrogen oxides in the troposphere: Global and regional budgets, *J. Geophys. Res.-Oceans*, 88, 10785-10807, doi:10.1029/JC088iC15p10785, 1983.
- Luo, G., Yu, F., and Moch, J. M.: Further improvement of wet process treatments in GEOS-Chem v12.6.0: Impact on global distributions of aerosols and aerosol precursors, *Geosci. Model Dev.*, 13, 2879-2903, doi:10.5194/gmd-13-2879-2020, 2020.
- 710 Marais, E. A., Jacob, D. J., Choi, S., Joiner, J., Belmonte-Rivas, M., Cohen, R. C., Beirle, S., Murray, L. T., Schiferl, L. D., Shah, V., et al.: Nitrogen oxides in the global upper troposphere: interpreting cloud-sliced NO<sub>2</sub> observations from the OMI satellite instrument, *Atmos. Chem. Phys.*, 18, 17017-17027, doi:10.5194/acp-18-17017-2018, 2018.
- 715 Marais, E. A., Roberts, J. F., Ryan, R. G., Eskes, H., Boersma, K. F., Choi, S., Joiner, J., Abuhassan, N., Redondas, A., Grutter, M., et al.: New observations of NO<sub>2</sub> in the upper troposphere from TROPOMI, *Atmos. Meas. Tech.*, 14, 2389-2408, doi:10.5194/amt-14-2389-2021, 2021.
- Marenco, A., Thouret, V., Nédélec, P., Smit, H., Helden, M., Kley, D., Karcher, F., Simon, P., Law, K., Pyle, J., et al.: Measurement of ozone and water vapor by Airbus in-service aircraft: The MOZAIC airborne program, an overview, *J. Geophys. Res.-Atmos.*, 103, 25631-25642, doi:10.1029/98jd00977, 1998.
- 720 Mickley, L. J., Murti, P. P., Jacob, D. J., Logan, J. A., Koch, D. M., and Rind, D.: Radiative forcing from tropospheric ozone calculated with a unified chemistry-climate model, *J. Geophys. Res.-Atmos.*, 104, 30153-30172, doi:10.1029/1999jd900439, 1999.
- Murray, L. T., Jacob, D. J., Logan, J. A., Hudman, R. C., and Koshak, W. J.: Optimized regional and interannual variability of lightning in a global chemical transport model constrained by LIS/OTD satellite data, *J. Geophys. Res.-Atmos.*, 117, doi:10.1029/2012jd017934, 2012.
- 725 Murray, L. T., Logan, J. A., and Jacob, D. J.: Interannual variability in tropical tropospheric ozone and OH: The role of lightning, *J. Geophys. Res.-Atmos.*, 118, 411468-411480, doi:10.1002/jgrd.50857, 2013.
- Murray, L. T., Fiore, A. M., Shindell, D. T., Naik, V., and Horowitz, L. W.: Large uncertainties in global hydroxyl projections tied to fate of reactive nitrogen and carbon, *P. Natl. Acad. Sci. USA*, 118, e2115204118, doi:10.1073/pnas.2115204118, 2021.
- 730 NASA, NASA: Airborne Science Data for Atmospheric Composition: <https://www-air.larc.nasa.gov/cgi-bin/ArcView/arctas?DC8=1>, [last accessed: 24 October], 2009.
- NASA, NASA: Airborne Science Data for Atmospheric Composition: <https://www-air.larc.nasa.gov/cgi-bin/ArcView/seac4rs>, [last accessed: 24 October], 2015.
- 735 NASA, NASA: EARTHDATA, Korea United States Air Quality Study: <https://asdc.larc.nasa.gov/project/KORUS-AQ>, [last accessed: 24 October], 2017.

- NASA, NASA: EARTHDATA, ATom: Merged Atmospheric Chemistry, Trace Gases, and Aerosols, Version 2: [https://daac.ornl.gov/cgi-bin/dsviewer.pl?ds\\_id=1925](https://daac.ornl.gov/cgi-bin/dsviewer.pl?ds_id=1925), [last accessed: 24 October], 2021.
- 740 Nault, B. A., Garland, C., Pusede, S. E., Wooldridge, P. J., Ullmann, K., Hall, S. R., and Cohen, R. C.: Measurements of  $\text{CH}_3\text{O}_2\text{NO}_2$  in the upper troposphere, *Atmos. Meas. Tech.*, 8, 987-997, doi:10.5194/amt-8-987-2015, 2015.
- Petzold, A., Thouret, V., Gerbig, C., Zahn, A., Brenninkmeijer, C. A. M., Gallagher, M., Hermann, M., Pontaud, M., Ziereis, H., Boulanger, D., et al.: Global-scale atmosphere monitoring by in-service aircraft – Current achievements and future prospects of the European Research Infrastructure IAGOS, *Tellus B*, 67, 28452, doi:10.3402/tellusb.v67.28452, 2015.
- 745 Pollack, I. B., Lerner, B. M., and Ryerson, T. B.: Evaluation of ultraviolet light-emitting diodes for detection of atmospheric  $\text{NO}_2$  by photolysis - chemiluminescence, *J. Atmos. Chem.*, 65, 111-125, doi:10.1007/s10874-011-9184-3, 2010.
- Prather, M. J., and Jacob, D. J.: A persistent imbalance in  $\text{HO}_x$  and  $\text{NO}_x$  photochemistry of the upper troposphere driven by deep tropical convection, *Geophys. Res. Lett.*, 24, 3189-3192, doi:<https://doi.org/10.1029/97GL03027>, 1997.
- 750 Rap, A., Richards, N. A. D., Forster, P. M., Monks, S. A., Arnold, S. R., and Chipperfield, M. P.: Satellite constraint on the tropospheric ozone radiative effect, *Geophys. Res. Lett.*, 42, 5074-5081, doi:10.1002/2015gl064037, 2015.
- Reed, C., Brumby, C. A., Crilley, L. R., Kramer, L. J., Bloss, W. J., Seakins, P. W., Lee, J. D., and Carpenter, L. J.: HONO measurement by differential photolysis, *Atmos. Meas. Techn.*, 9, 2483-2495, doi:10.5194/amt-9-2483-2016, 2016a.
- 755 Reed, C., Evans, M. J., Di Carlo, P., Lee, J. D., and Carpenter, L. J.: Interferences in photolytic  $\text{NO}_2$  measurements: explanation for an apparent missing oxidant?, *Atmos. Chem. Phys.*, 16, 4707-4724, doi:10.5194/acp-16-4707-2016, 2016b.
- 760 Roberts, J. M.: The atmospheric chemistry of organic nitrates, *Atmos. Environ. A-Gen.*, 24, 243-287, doi:10.1016/0960-1686(90)90108-Y, 1990.
- Roberts, J. M., Williams, J., Baumann, K., Buhr, M. P., Goldan, P. D., Holloway, J., Hübler, G., Kuster, W. C., McKeen, S. A., Ryerson, T. B., et al.: Measurements of PAN, PPN, and MPAN made during the 1994 and 1995 Nashville Intensives of the Southern Oxidant Study: Implications for regional ozone production from biogenic hydrocarbons, *J. Geophys. Res.-Atmos.*, 103, 22473-22490, doi:10.1029/98JD01637, 1998.
- 765 Roberts, J. M., Flocke, F., Stroud, C. A., Hereid, D., Williams, E., Fehsenfeld, F., Brune, W., Martinez, M., and Harder, H.: Ground-based measurements of peroxy-carboxylic nitric anhydrides (PANs) during the 1999 Southern Oxidants Study Nashville Intensive, *J. Geophys. Res.-Atmos.*, 107, ACH 1-1-ACH 1-10, doi:10.1029/2001JD000947, 2002.
- 770 Ryerson, T. B., Williams, E. J., and Fehsenfeld, F. C.: An efficient photolysis system for fast-response  $\text{NO}_2$  measurements, *J. Geophys. Res.-Atmos.*, 105, 26447-26461, doi:10.1029/2000JD900389, 2000.
- Schultz, M. G., Jacob, D. J., Wang, Y., Logan, J. A., Atlas, E. L., Blake, D. R., Blake, N. J., Bradshaw, J. D., Browell, E. V., Fenn, M. A., et al.: On the origin of tropospheric ozone and  $\text{NO}_x$  over the tropical South Pacific, *J. Geophys. Res.: Atmos.*, 104, 5829-5843, doi:10.1029/98jd02309, 1999.

- 775 Seltzer, K. M., Vizuite, W., and Henderson, B. H.: Evaluation of updated nitric acid chemistry on ozone precursors and radiative effects, *Atmos. Chem. Phys.*, 15, 5973-5986, doi:10.5194/acp-15-5973-2015, 2015.
- Shah, V., Jacob, D. J., Dang, R., Lamsal, L. N., Strode, S. A., Steenrod, S. D., Boersma, K. F., Eastham, S. D., Fritz, T. M., Thompson, C., et al.: Nitrogen oxides in the free troposphere: implications for tropospheric oxidants and the interpretation of satellite NO<sub>2</sub> measurements, *Atmos. Chem. Phys.*, 23, 1227-1257, doi:10.5194/acp-23-1227-2023, 2023.
- 780 Silvern, R. F., Jacob, D. J., Travis, K. R., Sherwen, T., Evans, M. J., Cohen, R. C., Laughner, J. L., Hall, S. R., Ullmann, K., Crounse, J. D., et al.: Observed NO/NO<sub>2</sub> Ratios in the Upper Troposphere Imply Errors in NO-NO<sub>2</sub>-O<sub>3</sub> Cycling Kinetics or an Unaccounted NO<sub>x</sub> Reservoir, *Geophys. Res. Lett.*, 45, 4466-4474, doi:10.1029/2018gl077728, 2018.
- 785 Singh, H. B.: Reactive nitrogen in the troposphere, *Environ. Sci. Technol.*, 21, 320-327, doi:10.1021/es00158a001, 1987.
- Singh, H. B., Thompson, A. M., and Schlager, H.: SONEX airborne mission and coordinated POLINAT-2 activity: Overview and accomplishments, *Geophys. Res. Lett.*, 26, 3053-3056, doi:10.1029/1999GL900588, 1999.
- 790 Singh, H. B., Brune, W. H., Crawford, J. H., Jacob, D. J., and Russell, P. B.: Overview of the summer 2004 Intercontinental Chemical Transport Experiment–North America (INTEX-A), *J. Geophys. Res.-Atmos.*, 111, doi:10.1029/2006JD007905, 2006.
- Singh, H. B., Brune, W. H., Crawford, J. H., Flocke, F., and Jacob, D. J.: Chemistry and transport of pollution over the Gulf of Mexico and the Pacific: spring 2006 INTEX-B campaign overview and first results, *Atmos. Chem. Phys.*, 9, 2301-2318, doi:10.5194/acp-9-2301-2009, 2009.
- 795 Sörgel, M., Regelin, E., Bozem, H., Diesch, J. M., Drewnick, F., Fischer, H., Harder, H., Held, A., Hosaynali-Beygi, Z., Martinez, M., et al.: Quantification of the unknown HONO daytime source and its relation to NO<sub>2</sub>, *Atmos. Chem. Phys.*, 11, 10433-10447, doi:10.5194/acp-11-10433-2011, 2011.
- Stettler, M. E. J., Eastham, S., and Barrett, S. R. H.: Air quality and public health impacts of UK airports. Part I: Emissions, *Atmos. Environ.*, 45, 5415-5424, doi:10.1016/j.atmosenv.2011.07.012, 2011.
- 800 Stratmann, G., Ziereis, H., Stock, P., Brenninkmeijer, C. A. M., Zahn, A., Rauthe-Schöch, A., Velthoven, P. V., Schlager, H., and Volz-Thomas, A.: NO and NO<sub>y</sub> in the upper troposphere: Nine years of CARIBIC measurements onboard a passenger aircraft, *Atmos. Environ.*, 133, 93-111, doi:10.1016/j.atmosenv.2016.02.035, 2016.
- 805 Talbot, R. W., Dibb, J. E., Scheuer, E. M., Kondo, Y., Koike, M., Singh, H. B., Salas, L. B., Fukui, Y., Ballenthin, J. O., Meads, R. F., et al.: Reactive nitrogen budget during the NASA SONEX Mission, *Geophys. Res. Lett.*, 26, 3057-3060, doi:10.1029/1999GL900589, 1999.
- The International GEOS-Chem User Community: <https://doi.org/10.5281/zenodo.4681204>, 2021.
- 810 Thomas, K., Berg, M., Boulanger, D., Houben, N., Gressent, A., Nédélec, P., Pätz, H.-W., Thouret, V., and Volz-Thomas, A.: Climatology of NO<sub>y</sub> in the troposphere and UT/LS from measurements made in MOZAIC, *Tellus B*, 67, 28793, doi:10.3402/tellusb.v67.28793, 2015.
- Thompson, C. R., Wofsy, S. C., Prather, M. J., Newman, P. A., Hanisco, T. F., Ryerson, T. B., Fahey, D. W., Apel, E. C., Brock, C. A., Brune, W. H., et al.: The NASA Atmospheric Tomography (ATom) Mission: Imaging the chemistry of the global atmosphere, *B. Am. Meteorol. Soc.*, 1-53, doi:10.1175/bams-d-20-0315.1, 2021.

- 815 Toon, O. B., Maring, H., Dibb, J., Ferrare, R., Jacob, D. J., Jensen, E. J., Luo, Z. J., Mace, G. G., Pan, L. L., Pfister, L., et al.: Planning, implementation, and scientific goals of the Studies of Emissions and Atmospheric Composition, Clouds and Climate Coupling by Regional Surveys (SEAC<sup>4</sup>RS) field mission, *J. Geophys. Res.-Atmos.*, 121, 4967-5009, doi:10.1002/2015jd024297, 2016.
- 820 Travis, K. R., Jacob, D. J., Fisher, J. A., Kim, P. S., Marais, E. A., Zhu, L., Yu, K., Miller, C. C., Yantosca, R. M., Sulprizio, M. P., et al.: Why do models overestimate surface ozone in the Southeast United States?, *Atmos. Chem. Phys.*, 16, 13561-13577, doi:10.5194/acp-16-13561-2016, 2016.
- Travis, K. R., Heald, C. L., Allen, H. M., Apel, E. C., Arnold, S. R., Blake, D. R., Brune, W. H., Chen, X., Commene, R., Crounse, J. D., et al.: Constraining remote oxidation capacity with ATom observations, *Atmos. Chem. Phys.*, 20, 7753-7781, doi:10.5194/acp-20-7753-2020, 2020.
- 825 Travis, K. R., Nault, B. A., Crawford, J. H., Bates, K. H., Blake, D. R., Cohen, R. C., Fried, A., Hall, S. R., Huey, L. G., Lee, Y. R., et al.: Impact of improved representation of VOC emissions and production of NO<sub>x</sub> reservoirs on modeled urban ozone production, *Atmos. Chem. Phys.*, 2024, 1-27, doi:10.5194/egusphere-2024-951, 2024.
- 830 Volz-Thomas, A., Berg, M., Heil, T., Houben, N., Lerner, A., Petrick, W., Raak, D., and Pätz, H. W.: Measurements of total odd nitrogen (NO<sub>y</sub>) aboard MOZAIC in-service aircraft: instrument design, operation and performance, *Atmos. Chem. Phys.*, 5, 583-595, doi:10.5194/acp-5-583-2005, 2005.
- Weinheimer, A. J., Walega, J. G., Ridley, B. A., Gary, B. L., Blake, D. R., Blake, N. J., Rowland, F. S., Sachse, G. W., Anderson, B. E., and Collins, J. E.: Meridional distributions of NO<sub>x</sub>, NO<sub>y</sub>, and other species in the lower stratosphere and upper troposphere during AASE II, *Geophys. Res. Lett.*, 21, 2583-2586, doi:10.1029/94GL01897, 1994.
- 835 Weinheimer, A. J.: Chemical Methods: Chemiluminescence, Chemical Amplification, Electrochemistry, and Derivation, in: *Analytical Techniques for Atmospheric Measurement*, 311-360, doi:10.1002/9780470988510.ch7, 2006.
- 840 Worden, H. M., Bowman, K. W., Kulawik, S. S., and Aghedo, A. M.: Sensitivity of outgoing longwave radiative flux to the global vertical distribution of ozone characterized by instantaneous radiative kernels from Aura-TES, *J. Geophys. Res.*, 116, doi:10.1029/2010jd015101, 2011.
- Zahn, A., Brenninkmeijer, C. A. M., Asman, W. A. H., Crutzen, P. J., Heinrich, G., Fischer, H., Cuijpers, J. W. M., and van Velthoven, P. F. J.: Budgets of O<sub>3</sub> and CO in the upper troposphere: CARIBIC passenger aircraft results 1997–2001, *J. Geophys. Res.-Atmos.*, 107, ACH 6-1-ACH 6-20, doi:10.1029/2001JD001529, 2002.
- 845